Received: 1 March 2023 | Revised: 8 May 2023 | Accepted: 11 May 2023

DOI: 10.1002/app.54223

RESEARCH ARTICLE

Journal of Applied Polymer Science WILEY

The role of post-cure cycle on the thermomechanical properties of soy-based polyurethane thermosets

Franco Armanasco[1,2] | **Sebastián D'hers**[2] | **Leonel Matías Chiacchiarelli**[1,2]

[1]Group of Science and Technology of Polyurethane Materials, Instituto de Tecnología de Polímeros y Nanotecnología, Buenos Aires, Argentina

[2]Departamento de Ingeniería Mecánica, Instituto Tecnológico de Buenos Aires, Buenos Aires, Argentina

Correspondence
Leonel Matías Chiacchiarelli, Group of Science and Technology of Polyurethane Materials, Instituto de Tecnología de Polímeros y Nanotecnología, CONICET-UBA, Av. Gral. Las Heras, Buenos Aires 2214, Argentina.
Email: lchiacchiarelli@itba.edu.ar

Funding information
Agencia Nacional de Investigación y Desarrollo, Grant/Award Number: PICT2015 N0475; Agencia Nacional de Promoción Científica y Tecnológica, Grant/Award Number: PIP 2015 N0425

Abstract

A systematic study of the post-cure cycle of soy-based polyurethane thermosets was conducted as a function of crosslinker content, post-cure temperature and time. An improvement of 207% of the flexural strength, up to 175 MPa, was measured by increasing the crosslinking content to 60 wt% and by using a post-cure cycle temperature of 110°C. Similarly, the flexural modulus also increased by 199%, up to 3.2 GPa, while maintaining a flexural strain to failure of 6.60%. In situ studies of the post-cure cycle using dynamical mechanical analysis revealed the interplay between the two interpenetrating polymer networks as a function of crosslinker content. At a crosslinker content below 40 wt%, two rubbery to glass transition temperatures (T_g) were found at 60 and 200°C, respectively. At 60 wt%, only one T_g at temperatures close to the degradation temperature was identified (250°C). Scanning electron microscope micrographs of the fracture surface revealed the formation of stress induced cracks which were mitigated through the use of a temperature stepped post-cure cycle. The formation of soft segments with high degradation temperatures (485°C) were revealed by thermogravimetric analysis, which can be attributed to the presence of additional covalent bonds such as allophanate and carbodiimide that were also identified through Fourier transform infrared analysis. The results revealed in this work are key for the development of biobased polyurethanes applied for the polymer composite industry. In this regard, this study represented the first analysis of the post-cure cycle of a soy-based polyurethane thermoset.

KEYWORDS

post-cure analysis, soy-based polyurethane, thermomechanical properties, thermoset

1 | INTRODUCTION

The polyurethane industry is shifting towards sustainable solutions that have a positive impact on the environment, economy, and society. Most polyurethanes are currently synthesized from nonrenewable resources, such as gas and fuel oil, but the use of renewable resources, particularly vegetable oils, has become a priority.[1] Within the Americas region, adding value to agricultural products, particularly soybean oil, has become a primordial goal for sustainable development. A key achievement in this regard has been the United States Department of Agriculture Biopreferred program.[2]

Research studies focusing on the application of soy-based polyols in polyurethanes have tackled the development of rigid and flexible foams as well as elastomers and thermoplastics, but very few on thermosets.[3–15] One of the most relevant applications of thermosets is within the polymer composites field, where high hydroxyl functionalities, low viscosities as well as a hydrophobic formulation are key aspects for a successful scale-up.[16] Our group recently published a chemorheological analysis of a polyurethane thermoset which complied such characteristics, finding as well that the cure of this system was dominated by vitrification effects.[17] The rubbery to glass transition (T_g) is a typical thermal transition found in polymers and it reduces drastically the cure kinetics during cure.[18] The role of the post-cure cycle on the thermomechanical properties of the resultant thermoset was not addressed. It is important to understand that the development of a matrix applied to the polymer composites field requires the development of both a cure and a post-cure cycle.[16]

The relationship between the thermomechanical properties of the thermosets and the complete cure-cycle is a key issue that needs to be studied in detail. Within literature, several studies can be found for other thermoset systems, particularly epoxies.[19–27] However, as the authors are concerned, no other study has dealt so far with the development of a complete cure cycle associated with polyurethane thermosets obtained from soybean oil.

It is known that one of the main disadvantages of polyurethane thermosets rely on the fact of the susceptibility of the precursors or "resins" to the formation of pores which can generate a strong deleterious effect on its mechanical properties.[28–30] In this regard, it is important to emphasize that polyols obtained from vegetable oils have the intrinsic advantage of having a higher hydrophobic character. By contrast, traditional polyether's are much more hydrophilic. The main issue with vegetable polyols is that the combination of a high hydroxyl functionality and low processing apparent viscosity is usually very difficult to attain.[17] In this regard, biobased crosslinkers, such as glycerin obtained from the transesterification of soybean oil,[31,32] can circumvent this issue. However, it might be argued that glycerin has a very hygroscopic nature, leading to the formation of pores. As far as the authors are concerned, no other previous study has dealt with the effect on increasing amounts of glycerin content on the porosity as well as the thermomechanical properties of the resultant thermoset.

In this work, several post-cure cycles were designed and tested by changing temperature, crosslinker content and time. Quasi-static flexural and tensile mechanical properties were measured to obtain the optimum post-cure cycle. Dynamical mechanical analysis (DMA) was used to have an in situ measurement of the storage modulus as well as the damping factor, measurements which are key for the bulk determination of the transition temperature (T_g). Scanning electron microscope (SEM) micrographs were used to evaluate porosity as a function of crosslinker content as well as the fractured surface of the quasi-static mechanical tests. Thermogravimetric analysis (TGA) was used to characterize the thermal degradation of the thermosets as a function of crosslinker content as well as to find the specific amount of soft and hard segments present in it. Fourier transform infrared (FTIR) and differential scanning calorimeter (DSC) analysis were employed to obtain the chemical bonds present in the microstructure and for a residual cure analysis as a function of crosslinker content.

2 | MATERIALS AND METHODS

2.1 | Materials and sample manufacture

A polymeric methylene diphenyl diisocyanate (pMDI), denominated commercially as Suprasec 5005 (Huntsman), with an isocyanate number (NCO) of 31.0 and a functionality of 2.70 was used to prepare all the samples. Before use, the pMDI was degassed using a dispermat vacuum mixer at a pressure of 3.0 mbar mixing simultaneously at 5300 rpm. Glycerin (Anedra, USP) with a functionality of 3.00 and a hydroxyl number (OH#) of 1800 $\text{mgKOH}\cdot\text{g}^{-1}$ was used after degassing in a vacuum mixer. Dibutyltin dilaurate (95%, Sigma Aldrich) was used as the catalyst (DBTDL). A soy-based polyol (ESOP) with an OH# of 137 $\text{mgKOH}\cdot\text{g}^{-1}$, a functionality of 2.90, a molecular weight of 697 Da and with fully secondary hydroxyl groups was synthesized using the procedure already reported in a previous work.[17] Further details of the physicochemical properties of this polyol can also be consulted there.

The thermosetting polyurethane formulations used in this work as well as the different post-cure cycles are reported in Table 1. For clarity issues, the amount of dibutyltin dilaurate (DBTDL) and the isocyanate index ($\text{NCO}_{\text{index}}$) used in all the formulations were removed from this table, but they were held fixed at 0.2 parts by weight (pbw) and 1.05 pbw for all the samples, respectively.

The formulations reported in Table 1 were used to manufacture eight plates using the casting method. After thorough degassing, the components denoted in Table 1 were mixed together using a dispermat mixer at 7.80×10^3 rpm for 2 min and hand casted in an open aluminum mold. This mold had dimensions of 180 mm length by 180 mm in width and 8.00 mm in height. The total amount of material (resin) was always fixed so as to yield plates with similar thicknesses. In this regard, the average thickness of the plates was 2.06 mm with a standard deviation of 2.89×10^{-4} m. Each plate was left to cure at ambient temperature (25°C) overnight and then

TABLE 1 Formulations and post-cure cycles used in this work.

Formulation	ESOP (pbw)	Isocyanate (pbw)	Glycerin (pbw)	Total cure time (h)	Dwell time (h)	Tc_{max} (°C)
TsPU-GLI20-TC70	1.00×10^{2}	1.26×10^{2}	2.00×10^{1}	3.00×10^{0}	1 at 5.00×10^{1}°C, 2 at 7.00×10^{1}°C	7.00×10^{1}
TsPU-GLI20-TC110	1.00×10^{2}	1.26×10^{2}	2.00×10^{1}	5.00×10^{0}	1 at 5.00×10^{1}°C, 1 at 7.00×10^{1}°C, 1 at 9.00×10^{1}°C, 2 at 1.10×10^{1}°C	1.10×10^{2}
TsPU-GLI20-TC130	1.00×10^{2}	1.26×10^{2}	2.00×10^{1}	5.00×10^{0}	1 at 5.00×10^{1}°C, 1 at 7.00×10^{1}°C, 1 at 9.00×10^{1}°C, 1 at 1.10×10^{1}°C, 1 at 1.30×10^{1}°C	1.30×10^{2}
TsPU-GLI20-TC150	1.00×10^{2}	1.26×10^{2}	2.00×10^{1}	6.00×10^{0}	1 at 5.00×10^{1}°C, 1 at 7.00×10^{1}°C, 1 at 9.00×10^{1}°C, 1 at 1.10×10^{2}°C, 1 at 1.30×10^{2}°C, 1 at 1.50×10^{2}°C	1.50×10^{2}
TsPU-GLI20-TC170	1.00×10^{2}	1.26×10^{2}	2.00×10^{1}	7.00×10^{0}	1 at 5.00×10^{1}°C, 1 at 7.00×10^{1}°C, 1 at 9.00×10^{1}°C, 1 at 1.10×10^{2}°C, 1 at 1.30×10^{2}°C, 1 at 1.50×10^{2}°C, 1 at 1.70×10^{2}°C	1.70×10^{2}
TsPU-GLI20-TC70-3	1.00×10^{2}	1.26×10^{2}	2.00×10^{1}	3.00×10^{0}	1 at 5.00×10^{1}°C, 2 at 7.00×10^{1}°C	7.00×10^{1}
TsPU-GLI20-TC70-5	1.00×10^{2}	1.26×10^{2}	2.00×10^{1}	5.00×10^{0}	1 at 5.00×10^{1}°C, 4 at 7.00×10^{1}°C	7.00×10^{1}
TsPU-GLI20-TC70-8	1.00×10^{2}	1.26×10^{2}	2.00×10^{1}	8.00×10^{0}	1 at 5.00×10^{1}°C, 7 at 7.00×10^{1}°C	7.00×10^{1}
TsPU-GLI10-TC110	1.00×10^{2}	1.26×10^{2}	1.00×10^{1}	4.00×10^{0}	1 at 5.00×10^{1}°C, 1 at 7.00×10^{1}°C, 1 at 9.00×10^{1}°C, 1 at 1.10×10^{2}°C	1.10×10^{2}
TsPU-GLI40-TC110	1.00×10^{2}	1.26×10^{2}	4.00×10^{1}	4.00×10^{0}	1 at 5.00×10^{1}°C, 1 at 7.00×10^{1}°C, 1 at 9.00×10^{1}°C, 1 at 1.10×10^{2}°C	1.10×10^{2}
TsPU-GLI60-TC110	1.00×10^{2}	1.64×10^{2}	6.00×10^{1}	4.00×10^{0}	1 at 5.00×10^{1}°C, 1 at 7.00×10^{1}°C, 1 at 9.00×10^{1}°C, 1 at 1.10×10^{2}°C	1.10×10^{2}

demolded. One of these plates was used for DMA analysis (see second paragraph of section 2.2) while the rest were subjected to post-cure cycles using a forced convection oven (Milab 101-2AB) at the conditions specified in Table 1. Even though the temperature set-up and control was performed by the oven, two thermocouples were added at the top and bottom surface of the plate, so as to corroborate that precise and identical post-cure cycles were performed.

As can be deduced from Table 1, the post-cure cycle followed temperature steps of approximately 20–30°C until reaching the final post-cure temperature. For example, for the case of the TsPU-GLI20-TC70, this meant that the sample was first subjected to an isotherm at 50°C for 2 h and then to another isotherm at 70°C for an additional 2 h. This procedure was important to avoid the generation of thermal stresses which might cause the premature propagation of cracks. Such an effect was already reported before.[6] Further details in this regard can be consulted in section 6.2.

2.2 | Sample characterization techniques

Quasi-static flexural mechanical tests were performed using an Instron 5985 equipped with a 2.50×10^5 N load cell and by following the guidelines of the standard ASTM D790. Five samples for each formulation (as reported in Table 1) were tested. The span to depth ratio was set to 16:1 and the crosshead speed was 1.00×10^{-4} m·min^{-1}. Quasi-static tensile mechanical tests were performed using an Instron 5985 equipped with a 2.50×10^5 N load cell and by following the guidelines of the standard ASTM D-638. Five Dumbbell shaped specimens were cut according to the specified dimensions stablished by the standard and the tests were performed at a crosshead speed of 1.00×10^{-3} m·min^{-1}. To exemplify, for the case of the TsPU-GLI20-TC70, the flexural and tensile samples were cut from a plate which was post-cured using the procedure indicated in Table 1, that is, the plate was first subjected to an isotherm at 50°C for 2 h and then to another isotherm at 70°C for an additional 2 h.

DMA was carried out using a Perkin & Elmer DMA 8000 equipment using the single cantilever bending fixture mode. The oscillation frequency was fixed at 1.00×10^0 Hz and the amplitude to 4.00×10^{-6} m. It was corroborated that the experiments fell within the linear elastic region using a strain scan at ambient temperature. At least three samples were used to corroborate the reproducibility of the results. The sample dimensions ranged at 1.00×10^{-4} m in length, 8.80×10^{-3} m in width and 1.80×10^{-3} m in thickness. It were cut using a numerical control router from the plate manufactured by the casting method and cured at ambient temperature (please see details of this procedure in the last paragraph of the previous section). Two successive thermal cycles were applied to each sample. The first one started at 25°C and went up to 180°C with a scan rate of 3.00°C·min^{-1} while the second one was identical except that the final temperature was 250°C. It is important to highlight that for temperatures around 200–250°C, thermal degradation was possible (see Section 5), hence, the maximum temperature of the first thermal cycle was selected to avoid this issue.

As we have already reported in a chemorheology study of this formulation,[17] the evolution of the conversion (cure) is very slow due to vitrification effects. Hence, it is important to analysis the post-cure residual heat flow, which is a measurement performed by DSC analysis so as to corroborate if the material has reached to the final conversion. In this work, post-cure residual heat flow analysis was performed using a TA instruments Q2000 DSC using the modulated mode and aluminum pans. Dynamic thermal cycles started at -2.0×10^1°C going up to 2.00×10^2°C at a scan rate of 2.00×10^0°C·min^{-1}. Sample mass was typically within the order of 1.00×10^{-4} g. The modulated mode was useful to discern between the reversible and nonreversible heat flow. Thermal transitions such as the heat flow evolved during cure are nonreversible. On the other hand, the rubbery to glass transition is a reversible one. Hence, by using modulated DSC it was possible to have a much better resolution of both phenomena.[33]

FTIR analysis spectra were obtained using a Shimadzu IRAffinity-1 preparing thin films with KBr mixtures at a 60/40 weight percentage of sample/KBr proportion. This ratio was slightly changed while changing the glycerin content. Each spectrum was obtained by recording 50 scans with a resolution of 4.00 cm^{-1} and at ambient temperature. The phenyl absorption band (centered at 1.59×10^3 cm^{-1}) was used to normalize each spectra. Atmospheric correction was applied used the internal standard of the IRAaffinity solution software.

Micrographic analysis was performed using a Zeiss EVO 10 SEM using polished acrylic included specimens. The samples were gold sputtered using a Polaron SEM coating unit (model E5100) with an intensity of 20 mA and a voltage of 2.2 kV for a time lapse of 50 s. All micrographs were analyzed at an electron high tension of 5.00 kV and by using the secondary electron detector. Porosity statistical analysis was performed using the ImageJ software, version 1.60. To avoid confusion, the electronic micrographs in this manuscript (such as Figure 5) do not contain the details of how that image was taken, such as voltage, working distance, and focus. The original micrographs which contain all the details can be downloaded from the Supporting Information.

As far as notation is concerned, the materials prepared in this manuscript are referred as TsPU-GLIX-TCY, where the *X* is associated to the crosslinker content and *Y* is associated to the post-cure cycle type (see Table 1). When a material is referred as TsPU-GLIXX, it meant that that material was only subjected to the cure cycle (explained above).

3 | RESULTS

3.1 | Quasi-static mechanical tests

3.1.1 | Flexural mechanical tests

The effect of increasing the maximum post-cure cycle temperature (Tc_{max}) on the flexural strength (σ_f), strain to failure (ε_f), and flexural modulus (E_f) are reported in Table 2 as well as depicted in Figure 1. The σ_f and the E_f as a function of Tc_{max} followed an identical trend with a monotonous increase up to a Tc_{max} of 150°C and a subsequent decrease for a Tc_{max} of 170°C. The maximum σ_f, which was 102 MPa, was measured at a Tc_{max} of 150°C. Similar values of σ_f were measured for a Tc_{max} within the range 110–150°C, indicating that it was not necessary to increase the post-cure temperature to 150°C to attain the maximum σ_f. A similar deduction can also be made from the evolution of E_f as a function of Tc_{max}. On the other hand, the ε_f followed a monotonous decrease as a function of increasing Tc_{max}, but with a substantial decrease at a Tc_{max} of 170°C. A final remark can be made on the standard deviation of the mechanical properties reported in Table 2. For the particular case of the lowest Tc_{max}, the standard deviation was higher with respect to all the other tested Tc_{max}.

The effect of increasing crosslinker concentration on the flexural strength (σ_f), strain to failure (ε_f), and flexural modulus (E_f) are reported in Table 3. In this analysis, the Tc_{max} was kept constant at 110°C. The σ_f had a monotonous increase as a function of increasing crosslinker concentration, reaching the highest value for the TsPU-GLI60-TC110. It is important to highlight that an improvement of +207%, reaching up to 175 MPa was attained taking the TsPU-GLI10-TC110 as the baseline. In a similar way, a similar increase of the E_f was also measured for increasing crosslinker concentrations. An improvement of +199%, reaching up to 3.20 GPa was measured. Finally, the ε_f decreased as a function of increasing crosslinker concentration, but to a lesser extent. In fact, a decrease of approximately 12.9% was measured comparing the TsPU-GLI60-TC110 with respect to the TsPU-GLI10-TC110.

To understand why the flexural mechanical properties changed as a function of Tc_{max}, it is important to highlight which were the possible physicochemical changes taking place within the microstructure of the thermosetting polyurethane studied in this work. The polyurethane tested in this work comprised an interpenetrating urethane network formed by two different oligomers, that is, the epoxidized soybean oil polyol (ESOP) and glycerin (GLI). The GLI contributed to a microstructure with a high crosslinking density, because of its high hydroxyl value and low molecular weight. On the other hand, the ESOP contributed to a less crosslinked microstructure, due to its low hydroxyl value and intermediate molecular weight. It is important to highlight that the hydroxyls present on each precursor compete to react with the isocyanate group, changing the overall cure kinetics of the thermoset polyurethane.[17,34,35] A very important aspect that our group has already studied is vitrification. As it has already been studied in our previous work, vitrification affected substantially the cure kinetics of this thermoset. Another relevant aspect is the possible crystallization of the soft segment during a post-cure cycle experiment.[36] It is known that high molecular weight polyurethane networks are prone to the formation of semicrystalline structures.[36] For the particular case of thermoplastic polyurethanes, this characteristic is also priory designed so as to achieve a thermoplastic behavior. However, due to the fact that the polyurethane system that we have developed has a relatively low molecular weight and medium to high crosslinking, we assume that this phenomena did not take place. From a chemical point of view, the formation of additional chemical bonds in addition to the urethane network can also occur. FTIR analysis was performed to further study this aspect

TABLE 2 The role of Tc_{max} on the flexural mechanical properties of the TsPU.

Sample	σ_f (MPa)	Strain to failure (%)	Flexural modulus (GPa)	Tc_{max} (°C)
TsPU-GLI20-TC70	$9.07 \times 10^1 \pm 9.06 \times 10^0$	$8.10 \times 10^0 \pm 8.47 \times 10^{-1}$	$1.73 \times 10^0 \pm 2.69 \times 10^{-1}$	7.00×10^1°C
TsPU-GLI20-TC110	$9.94 \times 10^1 \pm 6.23 \times 10^0$	$5.69 \times 10^0 \pm 6.15 \times 10^{-1}$	$2.14 \times 10^0 \pm 2.00 \times 10^{-2}$	1.10×10^2°C
TsPU-GLI20-TC130	$9.50 \times 10^1 \pm 1.38 \times 10^0$	$5.43 \times 10^0 \pm 1.62 \times 10^{-1}$	$2.03 \times 10^0 \pm 2.30 \times 10^{-2}$	1.30×10^2°C
TsPU-GLI20-TC150	$1.02 \times 10^2 \pm 2.16 \times 10^0$	$6.25 \times 10^0 \pm 3.39 \times 10^{-1}$	$2.09 \times 10^0 \pm 4.70 \times 10^{-2}$	1.50×10^2°C
TsPU-GLI20-TC170	$5.67 \times 10^1 \pm 7.06 \times 10^0$	$4.28 \times 10^0 \pm 6.01 \times 10^{-1}$	$1.49 \times 10^0 \pm 4.40 \times 10^{-2}$	1.70×10^2°C

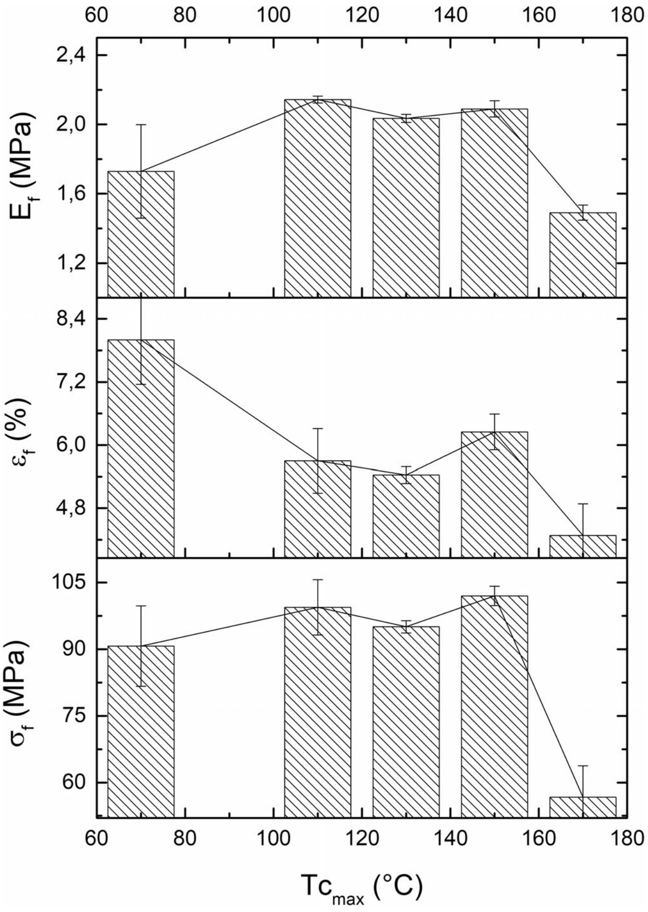

FIGURE 1 *Flexural* strength, elastic modulus, and strain to failure as a function of Tc_{max} for the TsPU-GLI20.

(see Section 7). Due to the fact that the polymer is being subjected to elevated temperatures, thermal degradation might also take place. Thermal degradation limits the maximum Tc_{max} that can be applied to the post-cure cycle. To this effect, further discussion on this regard can also be found in Section 5. Finally, defects such as porosity present in the thermoset can also cause a deleterious effect on the mechanical properties. In this regard, it is important to highlight that the post-cure was performed with isothermal stages separated at temperatures of approximately 20°C. This approach was a key aspect to avoid the formation and propagation of defects within the microstructure. Further details in this regard can be consulted in Section 6.

Taking into consideration the discussion on the previous paragraph, it can be concluded that the increase of both the σ_f and the E_f for a Tc_{max} up to 150°C (Figure 1) was mainly due to the formation of additional urethane bonds and an increase in crosslinking degree. However, for a Tc_{max} of 170°C, stress induced defects nucleating and propagating within the microstructure as well as thermal degradation caused a substantial decrease in the mechanical properties. The fact that the ε_f also decreased as a function of increasing Tc_{max} also supported this hypothesis.

As we have already emphasized in our previous work,[17] It is difficult to compare our results with previous studies. Studies of materials which are somehow similar to the one we reported can be consulted from Adekunle et al.[37,38] Nonetheless, it is important to emphasize that we can compare the thermomechanical properties of this polyurethane thermoset with other thermosets which are frequently employed in the polymer composite field, such as epoxies and polyesters. From Reference,[39] a fully diethylenetriamine cured epoxy material can achieve a σ_f between 1.00×10^8–1.20×10^8 Pa, an E_f of around 3.40 GPa and a maximum ε_f of 5.50%. For the case of high performance epoxy systems (such as the 3501-6 from Huntsman), Daniel and Ishai[40] reported similar values, with a higher E_f of 4.30 GPa. On the other hand, for polyester thermosets (unsaturated polyester resins), a typical σ_f ranges between 8.00×10^7 and 1.30×10^8 Pa, the E_f was around 3.50×10^9 Pa and the ε_f was below 3.30%.[41] Then, it can be concluded that the TsPU proposed in this work has the ability to compete with both systems and it has the advantage of having a higher ε_f, which, in turn, might lead to a tougher thermoset. In this section only the flexural properties have been compared. Nonetheless, similar conclusions can be made using the tensile properties reported in the subsequent section.

3.1.2 | Quasi-static tensile tests

The tensile strength (σ_t), tensile modulus (E_f), and tensile strain to failure (ε_t) as a function of increasing crosslinker content are reported in Table 4. Both the σ_t and the E_f followed a monotonous increase as a function of increasing crosslinker content, reaching the highest values for the TsPU-GLI60-TC110. Both the σ_t and the E_t had substantial increases of +253% and +276%, respectively, after increasing the crosslinker content from GLI10 to GLI60. On the other hand, the ε_t had only a slight decrease of 17.7% for that range.

The results outlined in this section support and validate the flexural properties which have been reported in section 3.1. Similar arguments than the ones described in this section can be used to understand the variation of the tensile properties as a function of crosslinker content.

4 | DYNAMICAL MECHANICAL THERMAL ANALYSIS

In the previous section, the effect of a specific post-cure cycle was quantified through the measurement of both

TABLE 3 TsPU flexural mechanical properties as a function of crosslinker content for a fixed Tc_{max} (1.10×10^{2}°C).

Sample	σ_f (MPa)	ε_f (%)	E_f (GPa)
TsPU-GLI10-TC110	$5.69 \times 10^{1} \pm 5.30 \times 10^{0}$	$7.59 \times 10^{0} \pm 7.16 \times 10^{-1}$	$1.07 \times 10^{0} \pm 1.42 \times 10^{-1}$
TsPU-GLI20-TC110	$9.94 \times 10^{1} \pm 6.23 \times 10^{0}$	$5.69 \times 10^{0} \pm 6.15 \times 10^{-1}$	$2.14 \times 10^{0} \pm 2.10 \times 10^{-2}$
TsPU-GLI40-TC110	$1.57 \times 10^{2} \pm 2.40 \times 10^{0}$	$6.50 \times 10^{0} \pm 2.81 \times 10^{-1}$	$2.84 \times 10^{0} \pm 3.40 \times 10^{-2}$
TsPU-GLI60-TC110	$1.75 \times 10^{2} \pm 4.12 \times 10^{0}$	$6.61 \times 10^{0} \pm 2.99 \times 10^{-1}$	$3.21 \times 10^{0} \pm 5.90 \times 10^{-2}$

TABLE 4 TsPU tensile mechanical properties as a function of crosslinker content.

Sample	Max. tensile strength (MPa)	Strain to failure (%)	Elastic modulus (GPa)
TsPU-GLI10-TC110	$2.38 \times 10^{1} \pm 1.85 \times 10^{0}$	$5.53 \times 10^{0} \pm 3.80 \times 10^{-1}$	$7.56 \times 10^{-1} \pm 4.90 \times 10^{-2}$
TsPU-GLI20-TC110	$4.77 \times 10^{1} \pm 2.98 \times 10^{0}$	$3.79 \times 10^{0} \pm 4.47 \times 10^{-1}$	$1.86 \times 10^{0} \pm 6.70 \times 10^{-2}$
TsPU-GLI40-TC110	$7.48 \times 10^{1} \pm 1.48 \times 10^{0}$	$4.77 \times 10^{0} \pm 3.87 \times 10^{-1}$	$2.61 \times 10^{0} \pm 4.80 \times 10^{-2}$
TsPU-GLI60-TC110	$8.40 \times 10^{1} \pm 7.50 \times 10^{-1}$	$4.55 \times 10^{0} \pm 2.23 \times 10^{-1}$	$2.84 \times 10^{0} \pm 5.60 \times 10^{-2}$

flexural and tensile mechanical tests. In this section, DMA thermal was implemented so as to obtain an in situ evolution of the storage modulus as well as the damping factor as a function of temperature.

The storage modulus (E') and the damping factor (Tan δ) as a function of temperature for the TsPUs with increasing amounts of crosslinker are depicted in Figures 2 and 3, respectively.

For the first thermal scan, the E' decreased sharply as a function of temperature (Figure 2a), regardless of crosslinker concentration. This suggested that the chemical conversion of all the formulations tested in this work were slow, a fact which can be ascribed to vitrification effects.[17] At a fixed temperature, the E' increased as a function of increasing crosslinker content, particularly for the formulations TsPU-GLI10, TsPU-GLI20, and TsPU-GLI40. In other words, the E' curve shifted upwards as a function of increasing crosslinker content. However, for the case of the TsPU-GLI60, a sharp and distinct decrease of the E' as a function of temperature (denoted by an arrow in Figure 2a) clearly disrupted this trend. For the case of the second thermal scan (Figure 2b), the decrease of E' as a function of temperature was much less pronounced, indicating the formation of a highly crosslinked network. The best performing formulation was the TsPU-GLI60, because the E' barely decreased as a function of temperature. It is important to highlight that, at temperatures above 200–250°C, all the formulations presented an abrupt decrease of E'. This result was expected due to the thermal decomposition of the hard segment (see Section 5). In addition, dimerization of isocyanate forming carbodiimide and gaseous CO_2 was also plausible (see Section 7).

The evolution of the damping factor as a function of temperature for the first thermal scan can be depicted in Figure 3a. In all cases, the damping factors had a strong increase at low temperatures, indicating the presence of a vitrified network. For example, for the case of the TsPU-GLI10, the damping factor increased substantially up to approximately 80°C, reaching a partial plateau which lasted up to 125°C, where a second rise was measured. This behavior can be ascribed to a network which is being cured, because the damping factor continuously increases as a function of increasing temperature. If the network had been completely crosslinked or cured, then, we would have measured a sharp increase and a subsequent decrease of the damping factor, whereas this maximum value would signal the location of a rubbery to glass transition temperature (T_g).

On the other hand, the second thermal scan (Figure 3b) presented a very distinct behavior. The damping factor presented two visible transitions which were dependent on the crosslinking content. The first transition, denoted as T_{g1} in Figure 3b, was centered at temperatures of approximately 60°C. Our group has already studied how this transition affected its cure kinetics.[17] However, in this work we have also studied the effect of increasing the crosslinker content on this transition. As it can be clearly noticed in Figure 3b, the transition (T_{g1}) is less pronounced as a function of increasing crosslinking content. The most compelling case was associated with the TsPU-GLI60, whereas the damping factor was the lowest and stayed at these levels up to temperatures well above 200°C. This clearly reflected the formation of a very crosslinked network with a very high transition temperature (denoted as T_{g2}), close to the degradation temperature.

A final remark about the specific value of the T_g as a function of increasing crosslinker content is worth mentioning. As can be deduced from Figure 3, the damping factor of the TsPU-GLI10, TsPU-GLI20, and TsPU-GLI40

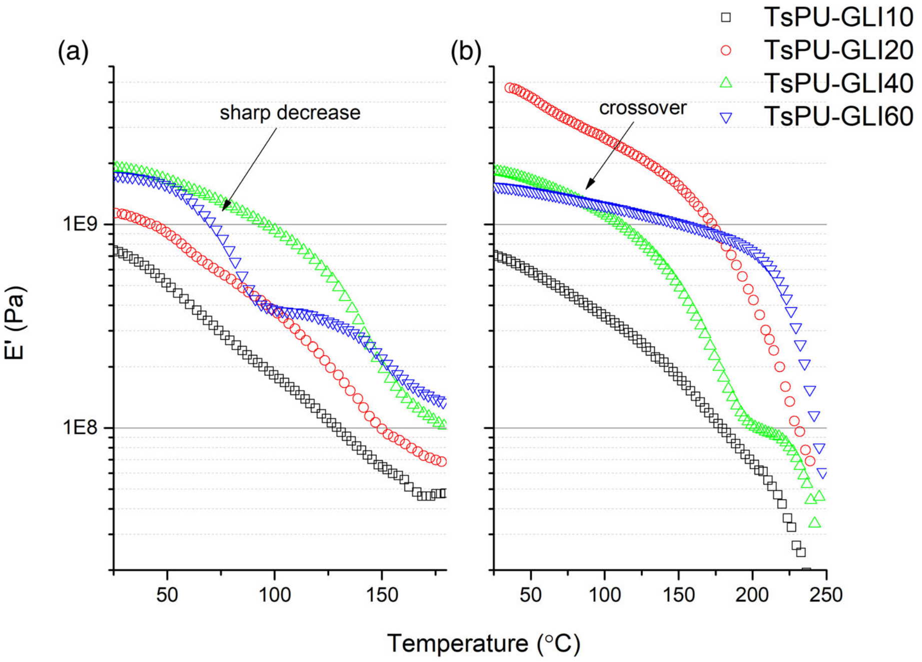

FIGURE 2 Storage modulus as a function of temperature and crosslinker content. (a) First thermal cycle and (b) second thermal cycle. [Color figure can be viewed at wileyonlinelibrary.com]

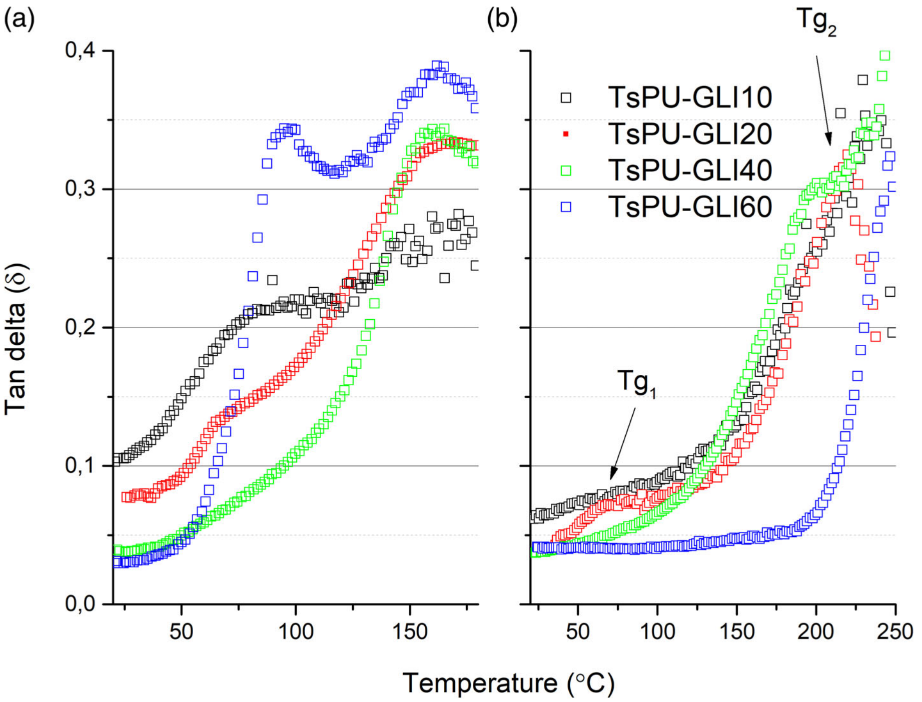

FIGURE 3 Damping factor as a function of temperature and crosslinker content. (a) First thermal cycle and (b) second thermal cycle. [Color figure can be viewed at wileyonlinelibrary.com]

had an important increase for temperatures above approximately 150°C. In typical thermoplastic polymers, the peak of the damping factor is usually ascribed to the T_g of the polymer network. However, in this case, we can only discern that the damping factor is reaching a transitory plateau. These results are coherent if we take into account that, for temperatures above 200–250°C, thermal degradation took place, hindering the formation of a maximum damping factor. In this case, the specific value of the T_g cannot be specified, but, instead, it can be argued that the T_g was very close to the degradation temperature of the polymer network, which was approximately 250°C. The evolution of the damping factor of the TsPU-GLI60 (Figure 3b) also supported this argument, whereas the damping factor maintained low values up to temperatures of approximately 200°C. Again, the formation of the damping factor peak was probably hindered due to the simultaneous degradation of the polymer network. In addition, other reactions might also take place, such as the dimerization of isocyanates, giving rise to carbodiimides. Please see Section 7 for further details in this regard.

In the previous results, the effect of post-cure temperature was evaluated. However, the effect of time is also relevant, because it might lead to a reordering of either the hard or soft segments.[36] As already noticed in Section 2, three cure cycles (TsPU-GLI20-TC70-3, TsPU-GLI20-TC70-5, and TsPU-GLI20-TC70-8) were performed at incremental times and those samples were subsequently analyzed in a conventional DMA thermal scan identical to the one outlined above. To avoid an extensive amount of figures in this manuscript, we have included the results in the supporting information. No significant changes were found in the thermomechanical properties of the samples analyzed, hence, it can be concluded that up to times of 7 h, no reordering of the microstructure of the polyurethane network took place. It is important to highlight that when time experiments are performed, specific cooling and heating rates have to be complied, otherwise, incoherent results may be the outcome of these measurements.

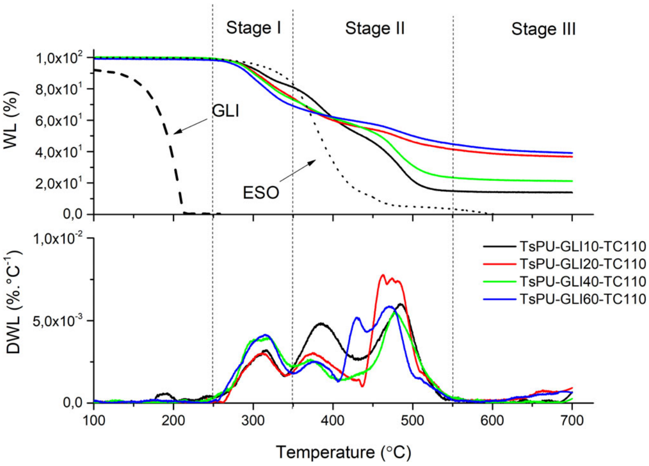

FIGURE 4 Weight loss and differential weight loss as a function of crosslinker content. [Color figure can be viewed at wileyonlinelibrary.com]

To sum up, the results in this section were the outcome of the complex cure of interpenetrating networks based on a polyol which had a mixture of low and medium molecular weight monomers in combination with moieties of very dissimilar reactivity. On one hand, the ESOP had the highest molecular weight and the lowest reactivity, because the hydroxyl functionality present in its structure was secondary. This gave rise to the formation of a network with a relatively low T_g, ranging at 60°C. On the other side, glycerin had a very low molecular weight and a higher reactivity, because the hydroxyls present within its chemical structure were of primary type. Even though the vitrification of one network affected the cure of the other network, very high T_g's, close to the degradation temperature, were attained by using a proper post-cure cycle.

5 | THERMAL DEGRADATION OF THE TSPUS (TGA)

The weight loss (WL) and the absolute value of its derivative (DWL) for the TsPUs as a function of increasing crosslinker content are depicted in Figure 4. As it is usually found for polyurethane materials, the degradation was divided into three stages.[4–6] Stage I covered the temperature region starting from 200°C and up to 350°C. In this stage, the decomposition of the urethane bond (hard segment) into alcohol, isocyanate, amines, and CO_2(g) took place.[42–45] As it can be deduced from Figure 4, a higher DWL and also WL was present as a function of increasing crosslinker content. Such a result was coherent because a higher content of crosslinker generated the formation of a higher concentration of urethane bonds within the material. Hence, it was coherent to expect a higher DWL as a function of increasing crosslinker content. Stage II covered the region between 350 and 550°C and it was associated

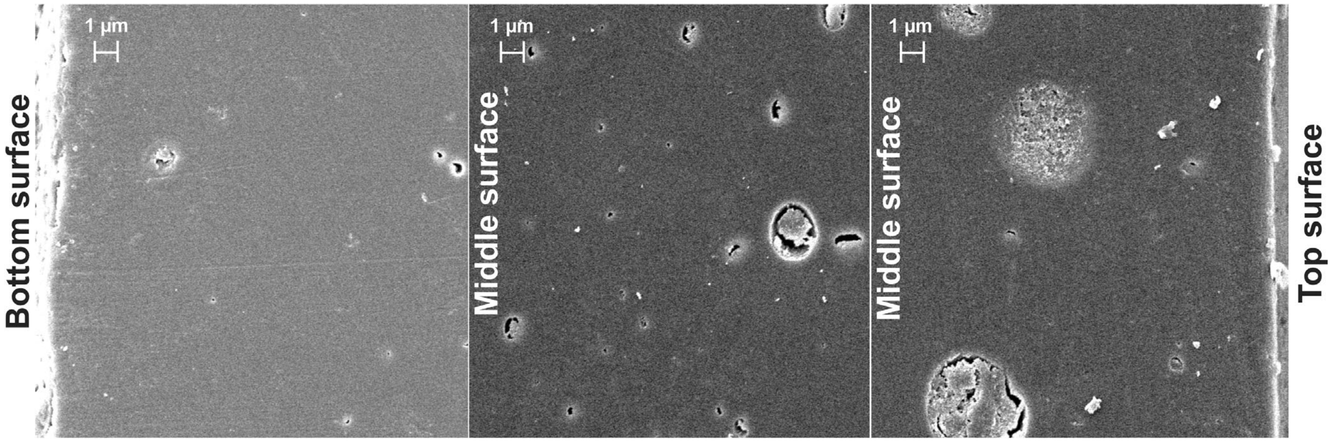

FIGURE 5 SEM micrographs of the through thickness porosity of a typical TsPU cured at TC110.

with the thermal decomposition of the soft segment. Within this stage, the DWL clearly indicated the presence of three degradation peaks which were centered at approximately 385, 430, and 485°C, respectively. These peaks were strongly dependent on crosslinker content. For the case of the peak centered at 385°C, the maximum DWL increased as a function of decreasing crosslinker content. This result suggested that the peak was associated with the thermal degradation of the ESOP. To further corroborate this hypothesis, the thermal degradation of the ESOP used in this work was also included in Figure 4. As it can be deduced, the peaks coincide, then, it can be asserted that the hypothesis was correct. In addition, the presence of this peak was also identified in previous studies.[6,7] On the other hand, peaks centered at higher temperatures (430 and 485°C) clearly indicated the formation of additional hard segments, which degrade at higher temperatures. However, a direct correlation with respect to crosslinker content was not found. These peaks might be associated with the degradation of additional covalent bonds, such as carbodiimide or allophanate, which were identified using FTIR analysis (see Section 7).

It is difficult to compare our results with previous studies. As far as the authors are concerned, no other work has dealt with this particular type of thermoset polyurethane. A recent study of Hojabri et al.[8] studying the thermal degradation of rigid polyurethane foams obtained from soy-based polyols and pMDI found peaks centered at temperatures of around 520°C. On the other hand, the early work of Fridrihsone et al.[6] found that polyols obtained from soy-based polyols had peaks centered at temperatures of approximately 410 and 480°C. Fu et al.[7] studied the thermal degradation of polyurethanes obtained from toluene diisocyanate and formiated soy-based polyols. The study revealed that the main peak was centered at a temperature of approximately 400°C. Javni et al.[9] studied the thermal degradation of rigid polyurethane foams obtained from a polyurea MDI prepolymer using soy-based polyols. All peaks were found for temperatures below 400°C. A recent study of Kirpluks et al.[10] found a peak centered at 461°C for the case of rigid polyurethane foams prepared from pMDI and formiated soy-based polyols.

6 | MICROSTRUCTURAL ANALYSIS

6.1 | Porosity

The sample porosity as a function of crosslinker concentration is reported in Table 5. As it can be deduced from the values, no correlation was found between porosity and crosslinker content. The highest porosity was 1.79% for the case of the TsPU-GLI40-TC110, but it changed slightly for all the other tested formulations. All the reported values in Table 5 clearly indicated that the samples were of very good quality and that porosity should not impose a problem for the development of soy-based polyurethanes thermosets.

TABLE 5 TsPU porosity as a function of crosslinker content.

Sample	Mean porosity (%)
TsPU-GLI10-TC110	$4.60 \times 10^{-1} \pm 3.00 \times 10^{-1}$
TsPU-GLI20-TC110	$1.25 \times 10^{0} \pm 1.20 \times 10^{-1}$
TsPU-GLI40-TC110	$1.79 \times 10^{0} \pm 6.00 \times 10^{-2}$
TsPU-GLI60-TC110	$1.06 \times 10^{0} \pm 4.40 \times 10^{-1}$

Taking into account that the sample was molded, one surface of the mold (bottom surface) was exposed to the aluminum mold while the other to air (top surface). Hence, it was coherent that the pores measured and reported in Table 5 might have a tendency to be found at the top surface of the mold. A typical set of figures which explains this effect can be depicted in Figure 5. The set of through thickness micrographs clearly indicated that the pores tended to accumulate near the top surface of the mold.

Within polyurethanes, it is well known that the presence of pores might have a detrimental effect on the mechanical properties. Pores can be formed by several mechanisms, the most important being the reaction of isocyanate with water, forming gaseous carbon dioxide.[46] However, this is usually the case when a hydrophilic polyol is used in the formulation of a polyurethane thermoset. For the case of conventional polyurethanes, the most important polyol used in thermosets is usually a polyether. However, this family of polyols is known to have a very high hydrophilic character, particularly when polyols with high hydroxyl value are used.[36] In the formulation proposed in our work, the polyol formulation is based mostly on a hydrophobic soy-based vegetable oil, which has a beneficial effect on not having significant water contents as well as a very low water uptake. However, as we have already mentioned above, we have incorporated glycerin in the formulation. Glycerin is known for its high hygroscopic character, but for the case presented in our work and as proven by the porosity values reported in Table 5, the incorporation of glycerin in the formulation did not have a significant deleterious effect.

6.2 | Post fracture surface analysis

The SEM micrographs showing the flexural induced fractured surface of the TsPU-GLI10-TC110, TsPU-GLI20-TC110, TsPU-GLI40-TC110, and TsPU-GLI60-TC110 are

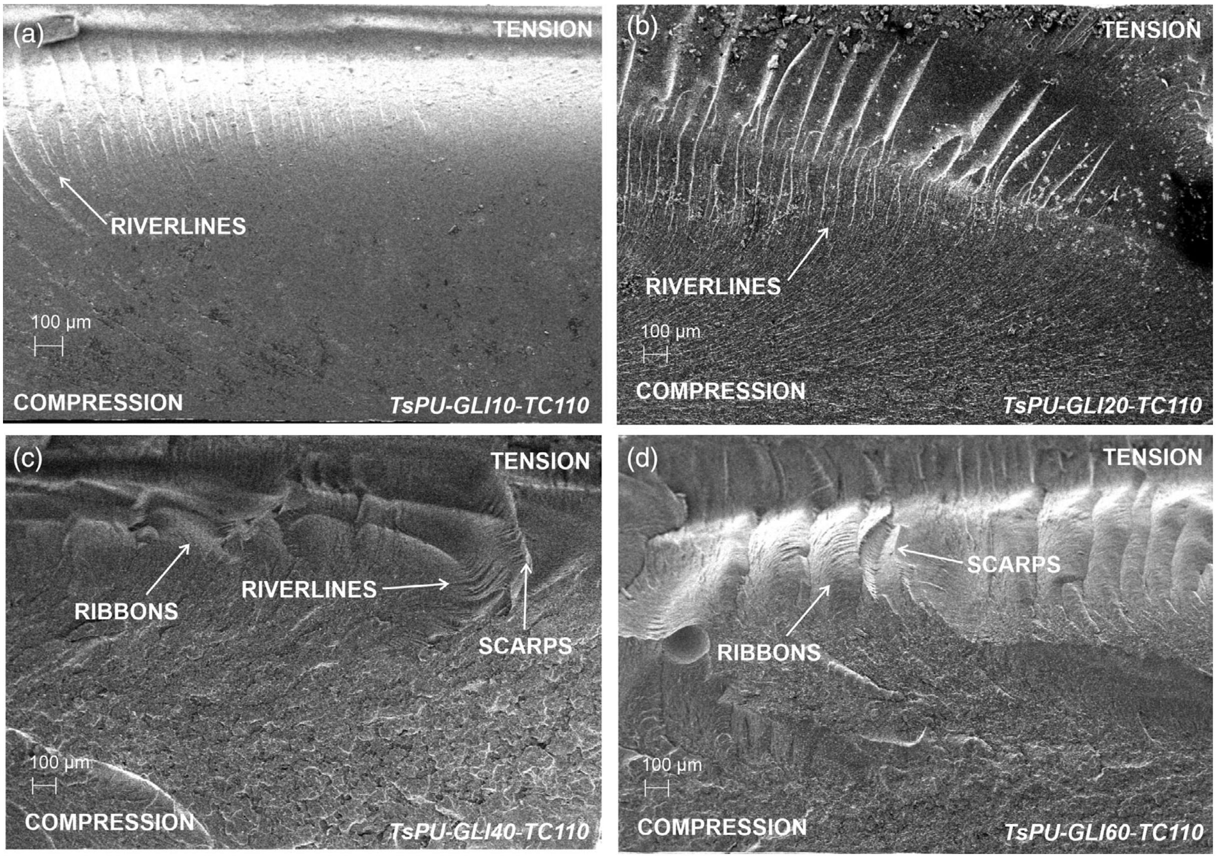

FIGURE 6 SEM micrographs of the fractured surface of the (a) TsPU-GLI10-TC110, (b) TsPU-GLI20-TC110, (c) TsPU-GLI40-TC110, and (d) TsPU-GLI60-TC110 samples.

depicted in Figure 6. Taking into account that a flexural state created both compressive and tensile states of stress, it was coherent to find dissimilar fracture surfaces delimited by the neutral axis. Specifically, all the figures presented in Figure 6 were arranged so that the top side represented the tensile state and the bottom side the compressive one. In addition, the figures were also arranged as a function of increasing crosslinker content, that is, GLI10 (Figure 6a), GLI20 (Figure 6b), GLI40 (Figure 6c), and GLI60 (Figure 6d), respectively.

For the case of the TSPU-GLI10-TC110, the micrographs showed mostly the presence of riverlines within the fracture surface. On the other hand, the TsPU-GLI60-TC110 presented the formation of riverlines, scarps, and ribbons. As already reported in previous studies,[47,48] such a change of the fracture surface was expected due to the change of the microstructure of the thermoset polyurethane. These results are in agreement with what would be expected for a polyurethane thermoset of these characteristics, whereas the fracture behavior was clearly dependent on crosslinker content.[49]

As previously described in the quasi-static mechanical tests (Section 3) and in particular in Table 2, a sharp decrease in flexural strength, flexural modulus, and flexural strain has been detected for all TSPU-GLI20 samples for post-cure cycles above 160°C. Micrographs of the fracture surface of those samples revealed the formation and propagation of cracks from seemingly spherical shaped defects, such as the ones depicted in Figure 7. Hence, it might be argued that the formation of those defects might be the cause of such detrimental effects on the mechanical properties. It is important to emphasize that at temperatures close to 200°C, the urethane group starts to decompose (see Section 5), hence, it might also be argued that thermal degradation might also have taken place. These temperatures may trigger additional reactions that generate CO_2(g), which can cause the formation of spherical defects in bulk. For example, isocyanate dimerization may occur, forming carbodiimides and releasing CO_2(g) as a byproduct.[36]

7 | INFRARED ABSORPTION ANALYSIS (FTIR)

The transmission spectra of the TsPUs developed in this work are depicted in Figure 8. In this graph, the absorption bands were identified and classified as a function of

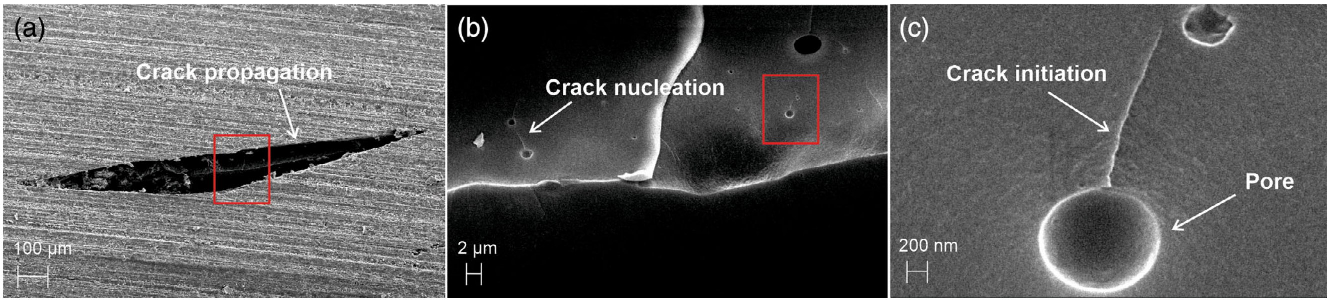

FIGURE 7 Electronic micrographs of crack initiation (c), nucleation (b), and propagation (a) of the TsPU-GLI20-TC170 samples. [Color figure can be viewed at wileyonlinelibrary.com]

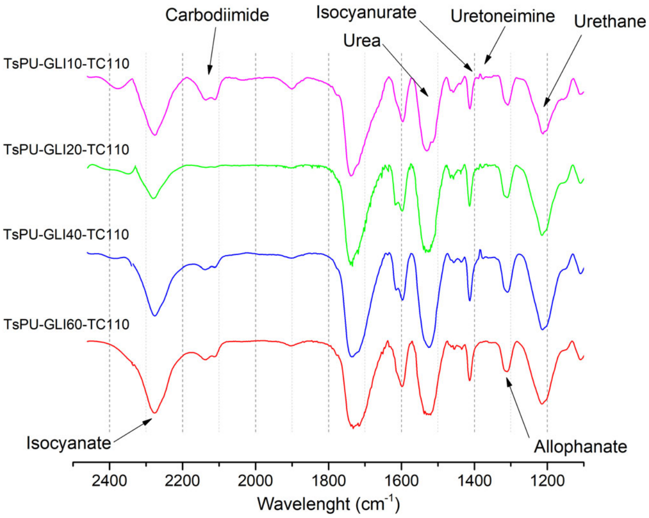

FIGURE 8 FTIR absorption spectra of the TsPU-TC110 samples as a function of crosslinker content. [Color figure can be viewed at wileyonlinelibrary.com]

increasing crosslinking content. The absorption band of the CO stretching of the urethane group was identified at 1220 cm^{-1}[50] and its variation as a function of crosslinking content was not significant. In a similar way, the absorption bands located at 1413 and 1510 cm^{-1} associated with the isocyanurate and urea group were also noticed.[50] On the other hand, the absorption bands of the isocyanate (2270 cm^{-1}), uretoneimine (1379 cm^{-1}), and carbodiimide (doublet at 2136 and 2100 cm^{-1}) groups had a significant variation as a function of crosslinking content.[36,50]

It is important to highlight that the isocyanate used in this work was a polymeric diphenylmethane diisocyanate (pMDI). Due to the fact that MDI is solid at room temperature, it is frequent to find eutectic variants[51] which are liquid at room temperature. To achieve this, the uretoneimine crosslinked structure is usually employed. However, it is known that the four member uretoneimine ring is thermally degraded for temperatures larger than 40°C.[51] This thermal degradation brings up the formation of equal molar quantities of isocyanate and carbodiimide groups. Due to the fact that the absorption bands of isocyanate, uretoneimine, and carbodiimide were clearly present in Figure 8, supporting the hypothesis that this phenomena might have taken place. This hypothesis was also reinforced because of the fact that all the materials presented in Figure 8 had post-cure treatments at temperatures well above 40°C. In this regard, it is important to bring to the discussion that the absorption bands of several groups tend to overlap. For example, within the region 1700–1750 cm^{-1}, the absorption bands of biuret, oxazolidone, isocyanurate carbonyl, and uretoneimine can certainly overlap. Hence, the hypotheses that are being developed have to be based on absorption bands where the overlap of several chemical groups is, ideally, absent. In this regard, the carbodiimide doublet found at 2136 and 2100 cm^{-1} as well as the isocyanate group (2270 cm^{-1}) can certainly be used to that effect. The doublet was found for all the formulations tested in this work, but it had the highest absorption for the TsPU-GLI10-TC110 and the minimum one for the TsPU-GLI20-TC110. Then, the hypothesis that the thermal degradation of the uretoneimine four ring member thermally degraded can be supported by this last experimental observation. In addition, the presence of isocyanate groups also reinforce this hypothesis. Particularly, it is important to notice that for the case of the TsPU-GLI20-TC110, which had the lowest carbodiimide absorption band had, in turn, the lowest isocyanate absorption band. These results are in agreement with what has already been found by Hatchett et al.[51] Another possible explanation of the formation of carbodiimides can also be ascribed to the dimerization of isocyanates.[36,52] This dimerization reaction might also induce the formation of carbon dioxide, which might induce an increased porosity (see Section 6).

Furthermore, the presence of an allophanate absorption band centered at approximately 1310 cm^{-1} clearly indicated the feasibility of reactions between isocyanates and urethanes. Such reactions might imply a more crosslinked structure. Nonetheless, no correlation between the formation of these bonds with crosslinker content was found.

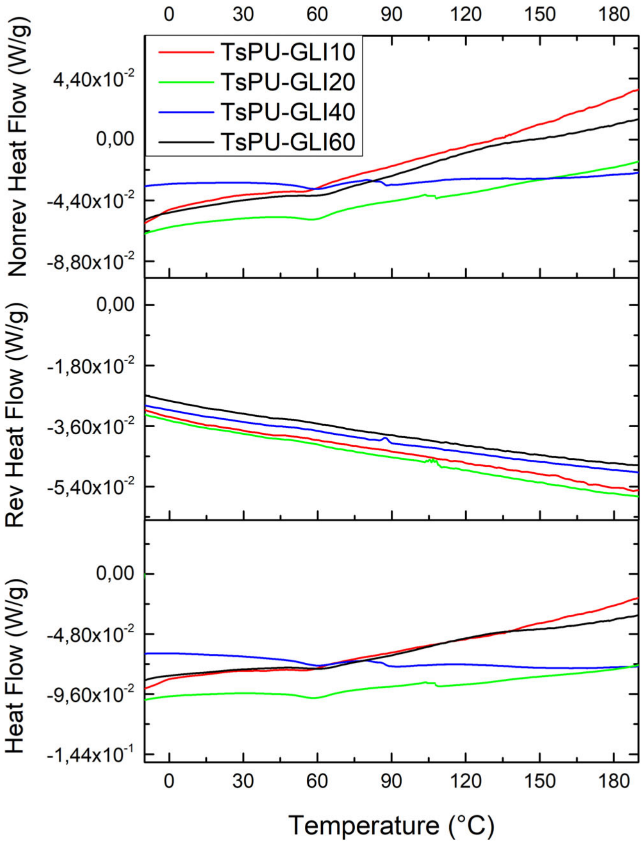

FIGURE 9 Heat flow, reversible heat flow, and nonreversible heat flow as a function of temperature for the TsPU-TC110. [Color figure can be viewed at wileyonlinelibrary.com]

In summary, the FTIR spectra corroborated the complex nature of the thermosetting polyurethane being studied in this work. The interplay between both interpenetrating networks and the formation of additional bonds which not only comprised urethane linkages but also allophanates as well as carbodiimides clearly reflected this complexity.

8 | RESIDUAL HEAT FLOW ANALYSIS OF POST-CURED SAMPLES

The total, reversible and nonreversible heat flow of the samples TsPU-GLI10-TC110, TsPU-GLI20-TC110, TsPU-GLI40-TC110, and TsPU-GLI60-TC110 as a function of temperature are depicted in Figure 9. To clarify, this heat flow was associated with post-cured samples, that is, the samples were first cured at room temperature and then post-cured at 110°C, as reported in Table 1.

The reversible heat flow indicated a T_g centered at approximately 40°C. The position of this thermal transition did not change noticeably as a function of crosslinker content. No other visible thermal transition was found, though the signal of the heat flow faintly reflected that a broad transition was present at higher temperatures.

The nonreversible heat flow indicated the presence of an enthalpic thermal transition which was centered at temperatures of approximately 60°C. The highest enthalpic transition was attributed to the TsPU-GLI60-TC110, at 1.02×10^1 J·g^{-1}, while the TsPU-GLI40-TC110 was 2.26×10^0 J·g^{-1}. The other samples presented a very small enthalpy which was considered very small to properly quantify. In addition, a change of slope was also observed at higher temperatures (as indicated by an arrow in Figure 9), but it was not possible to measure the enthalpic contribution due to the fact of not having a proper baseline to do it.

From this analysis it can be inferred that the residual heat flow of the samples post-cured at 110°C were either small or nonexistent, which served to conclude that the post-cure temperature was properly chosen. The enthalpic contributions presented in the previous paragraph were very small and it might not have a significant effect on the thermomechanical properties of a material subjected to that specific post-cure cycle. Another important deduction comes also by contrasting the results of this section and DMA analysis (Section 4). With DMA analysis it is possible to measure in a more accurate way how the thermal transitions directly affect the mechanical properties. On the other hand, even though we have employed a modulated DSC analysis, from the heat flow it was very difficult to properly discern the high temperature thermal transitions. A final remark has to be noticed about the position of the low temperature thermal transition. In this section, in the previous paragraph, it was asserted that the transition was centered at 40°C. On the other hand, in Section 4 (DMA analysis), the transition was measured at a higher temperature, that is, 60°C. At first sight, this might seem a contradiction, but, comparing the sample sizes of DMA and DSC analysis, it can be inferred that, for the former, thermal effects caused that temperature shift.

9 | CONCLUSIONS

An in depth study of the role of the post-cure cycle on the thermomechanical properties of a thermoset soy-based polyurethane was conducted. A temperature stepped post-cure cycle was found to avoid the formation of premature cracks (Section 6). The effect of increasing post-cure cycle temperature caused significant improvement of the quasi-static flexural and tensile mechanical properties. A temperature of 110°C produced the best improvement of mechanical properties, while for temperatures above 150–170°C, the mechanical properties were severely affected, probably because thermal stresses were induced by defects generated in the post-cure cycle. An excellent flexural strength of 175 MPa, flexural modulus of 3.20 GPa and flexural strain to failure of 6.60% was attained following the recommended post-cure cycle. Tensile properties of the samples also had a similar tendency. This clearly indicated that the proposed thermoset in this work can probably replace state of the art epoxy as well as polyester thermosets. TGA analysis revealed the formation of a SS with a high thermal degradation temperature of up to 485°C, suggesting the formation of a thermoset with an improved thermal degradation. FTIR analysis indicated the presence of not only traditional urethane bonds but, as well, allophanate and carbodiimide ones. DMA analysis revealed the presence of two thermal transitions, one centered at 60°C and another one which was highly dependent on crosslinker content. However, at a crosslinker content of 60 wt%, the most relevant thermal transition was centered at temperatures very close to the degradation temperature, that is, 250°C.

These results are of utmost importance for the development of biobased polyurethane thermosets applied mostly in the polymer composite industry. This study was the first one to disclose the role of the post-cure cycle on the thermomechanical properties of soy-based polyurethane thermosets and to develop a proper cure cycle which should be used in future research studies. Ongoing research in this area entails the manufacturing and characterization of polymer composites using this polymer as a matrix, particularly with flax, carbon and glass fiber reinforcements.

AUTHOR CONTRIBUTIONS

Franco Armanasco: Conceptualization (equal); data curation (lead); formal analysis (equal); investigation (equal); methodology (equal); writing – original draft (equal); writing – review and editing (equal). **Sebastián D'hers:** Funding acquisition (supporting); resources (supporting). **Leonel Matías Chiacchiarelli:** Conceptualization (lead); data curation (supporting); formal analysis (lead); funding acquisition (lead); methodology (lead); resources (lead); writing – original draft (lead); writing – review and editing (lead).

ACKNOWLEDGMENTS

The authors appreciate the advice and support from Matias Ferreyra (Huntsman), Edu Ruiz (POLYMTL) for his help with the modulated DSC analysis, Joaquin Infantino (ITBA) for SEM analysis and Hugo Nazareno Príncipe Lopez (ITPN) for its help with sample preparation. The work was funded by the "PICT 2015 N0475" ANPCYT (Argentina) as well as the "PIP-2015-N0425," supported by CONICET.

DATA AVAILABILITY STATEMENT

The data that supports the findings of this study are available in the supplementary material of this article.

ORCID

Franco Armanasco https://orcid.org/0000-0003-1221-2994
Sebastián D'hers https://orcid.org/0000-0002-4979-8813
Leonel Matías Chiacchiarelli https://orcid.org/0000-0002-7342-1784

REFERENCES

[1] C. Zhang, S. A. Madbouly, M. R. Kessler, *ACS Appl. Mater. Interfaces* **2015**, *7*, 1226.
[2] R. Buckhalt, *Ind. Biotechnol.* **2011**, *7*, 248.
[3] S. Anbinder, C. Meiorin, C. Macchi, M. A. Mosiewicki, M. I. Aranguren, A. Somoza, *Eur. Polym. J.* **2020**, *124*, 109470.
[4] J. M. Buffa, G. Mondragon, M. A. Corcuera, A. Eceiza, V. Mucci, M. I. Aranguren, *Eur. Polym. J.* **2018**, *98*, 116.
[5] M. Desroches, M. Escouvois, R. Auvergne, S. Caillol, B. Boutevin, *Polym. Rev.* **2012**, *52*, 38.
[6] A. Fridrihsone, F. Romagnoli, V. Kirsanovs, U. Cabulis, *J. Cleaner Prod.* **2020**, *266*, 121403.
[7] C. Fu, Z. Zheng, Z. Yang, Y. Chen, L. Shen, *Prog. Org. Coat.* **2014**, *77*, 53.
[8] L. Hojabri, X. Kong, S. S. Narine, *Biomacromolecules* **2009**, *10*, 884.
[9] I. Javni, Z. S. Petrović, A. Guo, R. Fuller, *J. Appl. Polym. Sci.* **2000**, *77*, 1723.
[10] M. Kirpluks, D. Kalnbunde, H. Benes, U. Cabulis, *Ind. Crops Prod* **2018**, *122*, 627.
[11] Y. Li, X. Luo, S. Hu, *Bio-Based Polyols and Polyurethanes*, Springer, Berlin **2015**, p. 15.
[12] S. Miao, P. Wang, Z. Su, S. Zhang, *Acta Biomater.* **2014**, *10*, 1692.
[13] Z. S. Petrović, *Polym. Rev.* **2008**, *48*, 109.
[14] S. Sahoo, H. Kalita, S. Mohanty, S. K. Nayak, *Int. J. Chem. Kinet.* **2016**, *48*, 622.
[15] Y. Xia, R. C. Larock, *Green Chem.* **2010**, *12*, 1893.
[16] P. Mallick, *Fiber-Reinforced Composites: Materials, Manufacturing, and Design*, 3rd ed., CRC press, New York **2007**.
[17] F. Armanasco, S. D'hers, L. Chiacchiarelli. *Kinetic and chemorheological modeling of thermosetting polyurethanes obtained from an epoxidized soybean oil polyol crosslinked with glycerin.* arXiv preprint arXiv:2204.07929. **2022**.
[18] D. I. Bower, *An Introduction to Polymer Physics*, Vol. 71, American Association of Physics Teachers, Cambridge **2003**, p. 285.
[19] L. P. Canal, M. Benavente, M. Hausmann, V. Michaud, *Compos. Part A: Appl. Sci. Manuf.* **2015**, *78*, 264.
[20] I. Hamerton, *High Perform. Polym.* **1996**, *8*, 83.
[21] F. Lionetto, A. Maffezzoli, *Materials* **2013**, *6*, 3783.
[22] W. Stark, H. Goering, U. Michel, H. Bayerl, *Polym. Test.* **2009**, *28*, 561.

[23] D. Lascano, L. Quiles-Carrillo, S. Torres-Giner, T. Boronat, N. Montanes, *Polymer* **2019**, *11*, 1354.

[24] P. P. Parlevliet, H. E. Bersee, A. Beukers, *Polym. Test.* **2010**, *29*, 291.

[25] R. Morales-Cerrada, R. Tavernier, S. Caillol, *Polymer* **2021**, *13*, 1255.

[26] O. Echeverria-Altuna, O. Ollo, I. Larraza, C. Elizetxea, I. Harismendy, A. Eceiza, *Polymer* **2022**, *14*, 4553.

[27] O. Yuksel, M. Sandberg, I. Baran, N. Ersoy, J. H. Hattel, R. Akkerman, *Compos., Part B* **2021**, *207*, 108543.

[28] M. Szycher, *Szycher's Handbook of Polyurethanes*, 2nd ed., CRC Press, New York **1999**.

[29] D. S. Kim, C. W. Macosko, *Polym. Eng. Sci.* **2000**, *40*, 2205.

[30] F. Yang, L. Cong, Z. Li, J. Yuan, G. Guo, L. Tan, *Constr. Build. Mater.* **2022**, *326*, 126784.

[31] L. Bournay, D. Casanave, B. Delfort, G. Hillion, J. A. Chodorge, *Catal. Today* **2005**, *106*, 190.

[32] A. Jaecker-Voirol, I. Durand, G. Hillion, B. Delfort, X. Montagne, *Oil Gas Sci. Technol.-Revue de l'IFP* **2008**, *63*, 395.

[33] B. H. Stuart, *Infrared Spectroscopy: Fundamentals and Applications*, John Wiley & Sons, Hoboken **2004**.

[34] L. M. Chiacchiarelli, J. M. Kenny, L. Torre, *Thermochim. Acta* **2013**, *574*, 88.

[35] J. M. E. Rodrigues, M. R. Pereira, A. G. Souza, M. L. Carvalho, A. A. D. Neto, T. N. C. Dantas, J. L. C. Fonseca, *Thermochim. Acta* **2005**, *427*, 31.

[36] M. Ionescu, *Chemistry and Technology of Polyols for Polyurethanes. Rapra Technologies*, 1st ed., Rapra Technology Limited, UK **2005**.

[37] K. Adekunle, D. Åkesson, M. Skrifvars, *J. Appl. Polym. Sci.* **2010**, *115*, 3137.

[38] K. Adekunle, S.-. W. Cho, R. Ketzscher, M. Skrifvars, *J. Appl. Polym. Sci.* **2012**, *124*, 4530.

[39] H. Dodiuk, *Handbook of Thermoset Plastics*, William Andrew, Amsterdam **2021**.

[40] I. M. Daniel, O. Ishai, *Engineering Mechanics of Composite Materials*, Vol. 3, Oxford University Press, New York **1994**.

[41] D. B. Miracle, S. L. Donaldson, S. D. Henry, C. Moosbrugger, G. J. Anton, B. R. Sander, N. Hrivnak, C. Terman, J. Kinson, K. Muldoon, *ASM Handbook*, Vol. 21, ASM International Materials Park, OH, USA **2001**.

[42] D. Chattopadhyay, D. C. Webster, *Prog. Polym. Sci.* **2009**, *34*, 1068.

[43] H. Hatakeyama, H. Matsumura, T. Hatakeyama, *J. Therm. Anal. Calorim.* **2013**, *111*, 1545.

[44] L. Jiao, H. Xiao, Q. Wang, J. Sun, *Polym. Degrad. Stab.* **2013**, *98*, 2687.

[45] L. L. Monteavaro, I. C. Riegel, C. L. Petzhold, D. Samios, *Polímeros* **2005**, *15*, 151.

[46] D. Randall, S. Lee, in *The Polyurethanes Book*, 2nd ed. (Eds: D. Randall, S. Lee), Wiley, New Jersey **2003**.

[47] R. V. Silva, D. Spinelli, W. W. Bose Filho, S. Claro Neto, G. O. Chierice, J. R. Tarpani, *Compos. Sci. Technol.* **2006**, *66*, 1328.

[48] C. McClory, T. McNally, G. P. Brennan, J. Erskine, *J. Appl. Polym. Sci.* **2007**, *105*, 1003.

[49] L. M. Chiacchiarelli, R. Petrucci, L. Torre, *Polym. Eng. Sci.* **2017**, *58*, 1241.

[50] M. Modesti, A. Lorenzetti, *Eur. Polym. J.* **2001**, *37*, 949.

[51] D. W. Hatchett, G. Kodippili, J. M. Kinyanjui, F. Benincasa, L. Sapochak, *Polym. Degrad. Stab.* **2005**, *87*, 555.

[52] J. Saunders, *Rubber Chem. Technol.* **1959**, *32*, 337.

SUPPORTING INFORMATION

Additional supporting information can be found online in the Supporting Information section at the end of this article.

How to cite this article: F. Armanasco, S. D'hers, L. M. Chiacchiarelli, *J. Appl. Polym. Sci.* **2023**, e54223. https://doi.org/10.1002/app.54223